

# UC Berkeley

## UC Berkeley Previously Published Works

### Title

A compact, high resolution energy, and emittance diagnostic for electron beams using active plasma lenses

### Permalink

<https://escholarship.org/uc/item/82s82496>

### Journal

Applied Physics Letters, 116(23)

### ISSN

0003-6951

### Authors

Barber, SK  
Bin, JH  
Gonsalves, AJ  
[et al.](#)

### Publication Date

2020-06-08

### DOI

10.1063/5.0005114

Peer reviewed

# A compact, high resolution energy, and emittance diagnostic for electron beams using active plasma lenses <sup>EP</sup>

Cite as: Appl. Phys. Lett. **116**, 234108 (2020); <https://doi.org/10.1063/5.0005114>

Submitted: 18 February 2020 . Accepted: 26 May 2020 . Published Online: 11 June 2020

<sup>id</sup> S. K. Barber, <sup>id</sup> J. H. Bin, <sup>id</sup> A. J. Gonsalves, F. Isono, <sup>id</sup> J. van Tilborg, <sup>id</sup> S. Steinke, <sup>id</sup> K. Nakamura, A. Zingale, N. A. Czaplá, D. Schumacher, <sup>id</sup> C. B. Schroeder, <sup>id</sup> C. G. R. Geddes, <sup>id</sup> W. P. Leemans, and E. Esarey

## COLLECTIONS

<sup>EP</sup> This paper was selected as an Editor's Pick



View Online



Export Citation



CrossMark

## ARTICLES YOU MAY BE INTERESTED IN

[Direct measurement of interfacial Dzyaloshinskii-Moriya interaction at the MoS<sub>2</sub>/Ni<sub>80</sub>Fe<sub>20</sub> interface](#)

Applied Physics Letters **116**, 232405 (2020); <https://doi.org/10.1063/5.0009828>

[Laser-heated capillary discharge plasma waveguides for electron acceleration to 8 GeV](#)

Physics of Plasmas **27**, 053102 (2020); <https://doi.org/10.1063/5.0002769>

[Perspectives on the generation of electron beams from plasma-based accelerators and their near and long term applications](#)

Physics of Plasmas **27**, 070602 (2020); <https://doi.org/10.1063/5.0004039>



Timing is everything.  
Now it's automatic.

A new synchronous source measure system for electrical measurements of materials and devices

**Lake Shore**  
CRYOTRONICS

[Learn more](#)

# A compact, high resolution energy, and emittance diagnostic for electron beams using active plasma lenses

Cite as: Appl. Phys. Lett. **116**, 234108 (2020); doi: [10.1063/5.0005114](https://doi.org/10.1063/5.0005114)

Submitted: 18 February 2020 · Accepted: 26 May 2020 ·

Published Online: 11 June 2020












View Online



Export Citation



CrossMark

S. K. Barber,<sup>1,a)</sup>  J. H. Bin,<sup>1</sup>  A. J. Gonsalves,<sup>1</sup>  F. Isono,<sup>1,2</sup> J. van Tilborg,<sup>1</sup>  S. Steinke,<sup>1</sup>  K. Nakamura,<sup>1</sup>   
A. Zingale,<sup>3</sup> N. A. Czaplá,<sup>3</sup> D. Schumacher,<sup>3</sup> C. B. Schroeder,<sup>1</sup>  C. G. R. Geddes,<sup>1</sup>  W. P. Leemans,<sup>1,b)</sup>   
and E. Esarey<sup>1</sup>

## AFFILIATIONS

<sup>1</sup>Lawrence Berkeley National Laboratory, Berkeley, California 94720, USA

<sup>2</sup>University of California, Berkeley, California 94720, USA

<sup>3</sup>The Ohio State University, Columbus, Ohio 43210, USA

<sup>a)</sup>Author to whom correspondence should be addressed: [sbarber@lbl.gov](mailto:sbarber@lbl.gov)

<sup>b)</sup>Present Address: Deutsches Elektronen-Synchrotron (DESY), Hamburg, Germany.

## ABSTRACT

High-resolution (sub-%), single-shot energy distribution, and emittance measurements of GeV-class electron beams generated by laser plasma accelerators (LPAs) have been enabled through the use of an active plasma lens combined with relatively short dipole magnets. This setup, with only 60 cm between the LPA source and the final diagnostic screen, was facilitated through the use of a replenishable  $\sim 20\text{--}40$  nm thick liquid crystal plasma mirror to separate remnant laser radiation from the electron beam without emittance degradation. As LPAs capable of generating GeV-class electron beams at cm-scale distances become increasingly ubiquitous, there is a need to supplement these compact accelerators with equally compact diagnostics.

Published under license by AIP Publishing. <https://doi.org/10.1063/5.0005114>

Plasma-based electron accelerators,<sup>1,2</sup> whether laser-driven or beam-driven, are now recognized by a rapidly expanding global community as a mature technology poised to support a host of applications. The ability of plasma-based accelerators to sustain  $>10$  GV/m acceleration gradients and to produce high-brightness GeV-class electron beams from cm-scale plasmas can enable radical reduction in the size of high impact light sources like x-ray free electron lasers (XFELs)<sup>3–5</sup> and monochromatic MeV photon sources based on Thomson scattering.<sup>6,7</sup> The compact nature of the plasma-based accelerator source could enable smaller laboratories, universities, hospitals, port authorities, and even mobile laboratories, to have access to a wide range of synchronized particles and radiation sources. Additionally, the plasma-based accelerator can form the fundamental building block for a future TeV electron-positron collider.<sup>8</sup>

While impressive progress in laser plasma accelerator (LPA) source development continues to be made, progress in complementary diagnostics specifically tailored to handle the unique properties and environments inherent to multi-GeV LPAs has not kept pace. When compared to conventional accelerators, the applicability of standard diagnostic techniques is hindered by the relatively large divergence

(mrad-level) and energy spread (few %) of the plasma-based accelerator.<sup>9</sup> Furthermore, the presence of high-intensity remnant laser radiation from the LPA source makes it difficult to introduce the auxiliary components (like, for example, electromagnets, integrating charge transformers, and scintillating screens) near the source. Consequently, the primary electron beam diagnostic for LPAs, the magnetic spectrometer, often relies on a simple design using a single magnetic dipole. In these geometries, achieving acceptable energy resolution can only come from the introduction of large energy dispersion and/or edge focusing effects.<sup>10</sup> For beams with energies in excess of 1 GeV, both these paths scale unfavorably and it becomes necessary to use configurations that rely on large drift distances and multi-ton electromagnets.<sup>11</sup>

Here, we present and experimentally demonstrate a compact magnetic spectrometer, combining short permanent magnet dipoles with high-gradient active plasma lens (APL) technology.<sup>12,13</sup> The radially symmetric focusing from the APL-enabled sub-% energy resolution and single-shot emittance studies at GeV-class energies is easily scalable toward 10 GeV and higher. The entire setup, from the LPA source to the diagnostic screen, is less than 65 cm in length, and all the hardware combined weighs on the order of 10 kg. The diagnostic is

positioned on translation stages for on-demand insertion and retraction, while the tunability of the APL allows for high energy resolution in a chosen beam energy range. The diagnostic was installed on the PetaWatt LPA<sup>14</sup> at the BELLA Center, measuring 4–5  $\mu\text{m}$  normalized beam emittances from an ionization injection-based LPA. The setup includes 10–100 nm thick liquid crystal films, acting as a plasma mirror (LCPM)<sup>15</sup> for removal of remnant LPA laser radiation without inducing emittance degradation typically associated with alternative replenishable multi-micrometer thick tape-based plasma mirrors.

The design of this diagnostic is based on standard electron beam optics<sup>16</sup> in which the transverse size of a beam is described in terms of the Twiss parameters, i.e.,  $\sigma = \sqrt{\beta \epsilon_n / \gamma_0}$ , where  $\beta$  is the beta function of the beam,  $\epsilon_n$  is the normalized emittance, and  $\gamma_0$  is the relativistic Lorentz factor. This expression excludes any terms related to energy spread of the beam. If, for example, the beam passes through a dipole, it will induce energy-dependent dispersion  $\eta$ , which contributes to the beam size in the bend plane as follows:  $\sigma = \sqrt{\beta \epsilon_n / \gamma_0 + (\eta \sigma_\gamma)^2}$ , where  $\sigma_\gamma$  is the relative energy spread of the beam. From this expression, it is clear that in order for a magnetic spectrometer to provide useful information about the energy content of a charged particle beam, the second term in the square root must dominate,  $\eta \sigma_\gamma > \sqrt{\beta \epsilon_n / \gamma_0}$ . Or to put it another way, the energy resolution of a magnetic spectrometer scales with  $\eta^{-1} \sqrt{\beta \epsilon_n / \gamma_0}$ .

To achieve high energy resolution, one can introduce large  $\eta$  and/or minimize  $\beta$  by focusing the beam. However, focusing GeV-class electron beams from an LPA presents some challenges for conventional charged particle focusing systems, which generally consist of electromagnetic (EMQ) or permanent magnet-based quadrupoles (PMQs). As an alternative to standard quadrupole focusing, the APL<sup>12,13</sup> has drawn considerable attention as it can provide tunable, multi kT/m, and radially symmetric focusing fields over 10's of cm of length with a compact transverse form factor. These characteristics of APLs make them considerably more attractive for short focal length focusing systems compared to conventional EMQ- or PMQ-based focusing.<sup>17</sup> The APL was instrumental in recent experiments demonstrating multi-stage acceleration of LPAs<sup>18</sup> and is regularly proposed as a potential solution for compact and emittance preserving transport in plasma-based accelerators.<sup>19–23</sup>

All these features of APLs make them an excellent choice for the development of a compact magnetic spectrometer. In particular, they make it possible to achieve low magnification of the electron source with short focal length lenses even at high energies. In such a configuration, the intrinsically small transverse source sizes of an LPA ( $\lesssim 10 \mu\text{m}$ ) can be directly translated to a location immediately downstream of the source. As noted above, a small focused spot size greatly reduces the dispersion needed to achieve high energy resolution for magnetic spectrometer applications. Thus, the dispersive element itself can be a relatively small. Before presenting the experimental demonstration, we first discuss practical design considerations for this type of spectrometer. In particular, for typical LPA sources, the chromatic focusing effects play an important role in determining the necessary dispersion.

The transfer matrix,  $R$ , for a simple focusing system consisting of a single thin lens with the imaging condition satisfied ( $R_{12} = 0$ ) is given by

$$R = \begin{pmatrix} -\frac{f_0}{d_0 - f_0} & 0 \\ -\frac{1}{f_0} & 1 - \frac{d_0}{f_0} \end{pmatrix}, \quad (1)$$

where  $d_0$  is the distance from the source to the lens,  $f_0$  is the focal length of the lens for electrons with a relativistic Lorentz factor of  $\gamma_0$ , and the spatial magnification of the system is given by the  $R_{11}$  element,  $M = \frac{f_0}{d_0 - f_0}$ . The description thus far does not include energy-dependent effects. These are included by generalizing the transfer matrix for the arbitrary Lorentz factor by substituting  $f_0$  with  $f = f_0(1 + \delta\gamma/\gamma_0)$ , where  $\delta\gamma/\gamma_0 = (\gamma - \gamma_0)/\gamma_0$  is the energy deviation from the nominal energy. Using the standard Twiss description, the beam size at the nominal image plane as a function of  $\delta\gamma/\gamma_0$  can be written as

$$\sigma_f(\delta\gamma/\gamma_0) = \sqrt{R_{11}^2 \sigma_0 + R_{12}^2 \sigma_0'}, \quad (2)$$

where  $\sigma_0$  and  $\sigma_0'$  are the initial source size and divergence, respectively. We have taken the reasonable approximation that the electron beam at the source location is near a waist ( $\alpha_0 \approx 0$ ), and note that variations in the virtual source location have a small impact on the overall results.

The impact of the initial e-beam parameters is illustrated in Fig. 1 in which we plot  $\sigma_f$  for various  $\sigma_0$  and  $\sigma_0'$  values using  $f_0 = 13 \text{ cm}$  and  $d_0 = 22 \text{ cm}$ . In Fig. 1(a),  $\sigma_0'$  is kept constant and  $\sigma_0$  is varied, while in (b),  $\sigma_0$  is fixed and  $\sigma_0'$  is varied. From these plots, it is clear that the beam size at  $\sigma_f(0)$  is independent of  $\sigma_0'$ , which makes intuitive sense since this is the energy for which the imaging condition is satisfied. Conversely, for values far from  $\delta\gamma/\gamma_0 = 0$ ,  $\sigma_f$  becomes independent of  $\sigma_0$  and is linearly dependent on  $\delta\gamma/\gamma_0$ , which is an important observation. If the beam size increase as a function of  $\delta\gamma/\gamma_0$  is larger than  $\eta$ , the different energies will not be cleanly separated and the energy resolution is impacted. For an e-beam with relatively small energy spread and a spectrometer with low chromaticity, as can be found in many conventional rf-based accelerators, this issue does not typically arise. To establish a criterion for which the spectrometer resolution is not unduly affected by this chromatic focusing effect, an expression for the slope of  $\sigma_f$  for  $\delta\gamma/\gamma_0 > 0$  can be derived and compared with the dispersion,

$$\left| \frac{d\sigma}{d\delta\gamma/\gamma_0} \right| \approx \frac{(M+1)^2}{M} f_0 \sigma_0' < \eta. \quad (3)$$

This condition indicates that the ideal geometry to reduce the required dispersion is one-to-one imaging using a short focal length lens, conditions best handled by an APL.

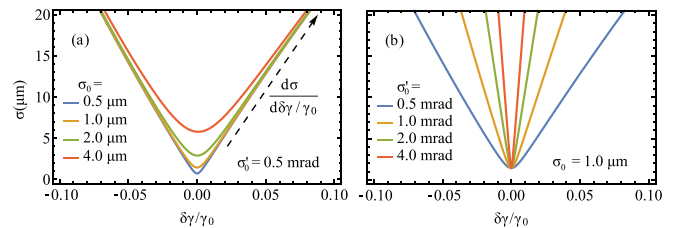


**FIG. 1.** Energy-dependent beam size for a simple imaging setup for beams with fixed initial source divergence and varying source sizes (a) and fixed source size and varying source divergence (b).

Using the above framework, we designed a spectrometer that would fit in the BELLA petawatt (PW) target chamber (i.e.,  $\sim 65$  cm long) and provide sub-% level resolution for the nominal case of 1 GeV electron beams with divergence up to 1 mrad. To meet the focusing requirements, we used a six cm long APL with a diameter of  $500 \mu\text{m}$  that is pulsed with a discharge current that reaches 570 A and decays to 0 A over 380 ns. The peak current of 570 A, combined with the APL geometry, indicates a maximum focusing gradient of 1800 kT/m and the effective focal length as short as 3 cm for 1 GeV electrons. By adjusting the time of arrival of the e-beam relative to the discharge, the focusing strength experienced by the beam can be easily adjusted. A schematic of the experiment is shown in Fig. 2.

For a dispersive element, we used a pair of 10 cm long permanent magnet dipoles with a peak field of 0.9 T. In principle, only a single dipole is needed. However, in order to minimize the impact on existing radiation safety protocols, we opted to use a pair of dipoles with opposite polarity (a so-called dogleg). A simple two dipole dogleg introduces an energy-dependent transverse offset with no residual angular kick, which is required to ensure that the beam hits the beam dump located  $> 10$  m downstream. The dispersion introduced by a dogleg with little to no drift between the dipoles can be approximated by  $\eta_x \approx 600 L_{\text{mag}}^2 B_z / \gamma_0$ , where  $L_{\text{mag}}$  is the length of the dipoles and  $B_z$  is the dipole magnetic field, which, for this dogleg, implies  $\eta = 2.8$  mm for the nominal case. A  $100 \mu\text{m}$  thick YAG:Ce crystal is located 2.5 cm downstream of the exit of the second dipole. The crystal is imaged at normal incidence using a  $5\times$ , infinite conjugate objective that is relay imaged out of vacuum, providing an optical resolution of  $3 \mu\text{m}$ . Due to the depth of field effects and the thickness of the YAG:Ce crystal, resolution of the electron beam is limited to  $7 \mu\text{m}$ . The YAG:Ce screen and imaging optics are mounted on the stage that translates in the bend plane, making it possible to scan the energy window viewed by the diagnostic. Ultimately, layout constraints imposed by the dogleg dictated a 1.75:1 magnification with a focal length of 14 cm, which, for the nominal case, equates to  $\frac{d\sigma}{d\delta\gamma/\gamma_0} = 600 \mu\text{m}$ , four times less than  $\eta$ , thus satisfying Eq. (3).

This experiment was performed at the BELLA Center using the PW laser system, which was tuned to produce 10 J on the target with a

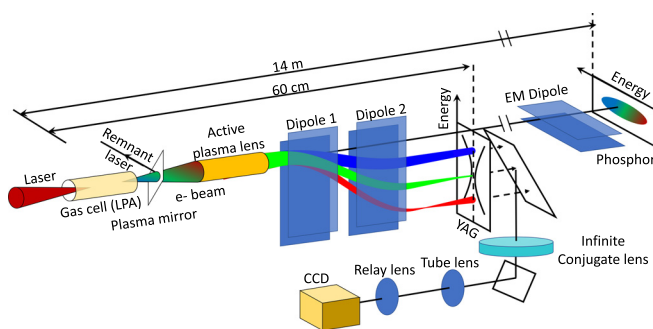


**FIG. 2.** Schematic representation of the experimental setup. The focused laser generates and accelerates electron beams in a gas cell, after which the laser is redirected with a plasma mirror to separate it from the electron beam and prevent damage to downstream components. An APL focuses the electron beam before it passes through a two-dipole dogleg to introduce dispersion. The different energies are focused uniquely, resulting in a characteristic bowtie shape that is incident upon an YAG:Ce screen, which is imaged onto a CCD. The YAG:Ce screen and dogleg are mounted on the translation stage, allowing them to be removed to establish baseline operation of the LPA using a calibrated magnetic spectrometer located 13 m downstream.

peak power of 0.25 PW and a peak intensity of  $4 \times 10^{18} \text{ W/cm}^2$ . The laser is focused onto a gas cell target filled with a mixture of 99% helium and 1% nitrogen with an average density of  $1.3 \times 10^{18} \text{ cm}^{-3}$ . Initially, the dogleg and YAG:Ce screen are removed from the beam-line to establish baseline operation of the LPA using an existing calibrated magnetic spectrometer<sup>24</sup> located 13 m downstream of the target. Quasi-monoenergetic electron beams with an average central energy of 840 MeV with an rms shot-to-shot jitter of 100 MeV and an rms energy spread of 265 MeV are generated. A representative single shot measurement of the electron beam energy spectrum is shown in Fig. 3(g).

To focus these beams onto the compact spectrometer YAG:Ce screen, we calculate the required discharge current of the APL. Because the APL is filled with hydrogen at 10 Torr, we note that the discharge current will tend to concentrate on the axis,<sup>25</sup> rather than be uniformly distributed over the APL aperture, resulting in an on-axis focusing enhancement of roughly 20%. Taking this into account, the desired current is around 80 A. We note that the same effect, which is related to temperature gradients in the plasma, leads to nonlinear focusing that focuses away from the axis, which can negatively impact the emittance of the beam. This point is discussed in the context of this diagnostic later in this Letter.

The compact spectrometer is then positioned such that the imaged portion of the YAG screen is centered on 850 MeV, as determined by the dispersion of the dogleg (which is 4 mm at 850 MeV). Several shots are shown in Figs. 3(a), 3(c), and 3(e), illustrating the effectiveness of the diagnostic. The beam in the dispersed direction is over 2 mm wide, but only tens of  $\mu\text{m}$  in the nondispersed direction. The absolute energy scale, which is determined only by the dispersion

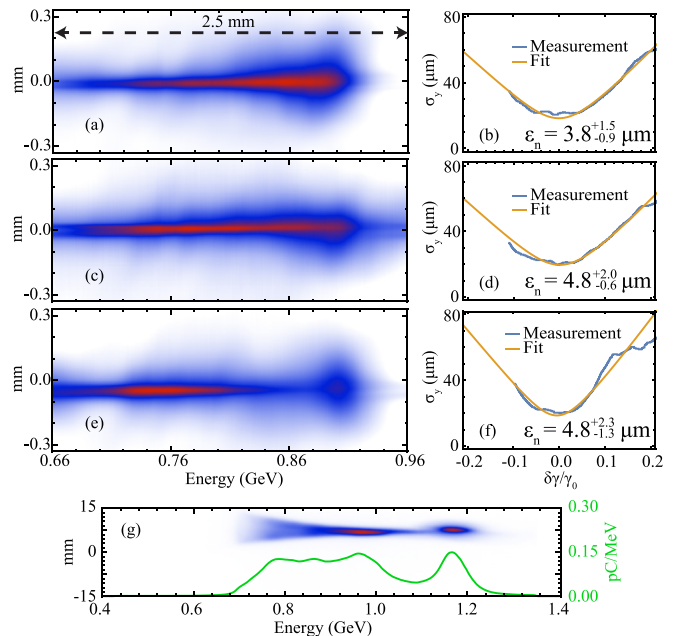


**FIG. 3.** Measured energy spectra measured using a compact magnet spectrometer (a), (c), and (e). Energy resolved beam size with fits to Eq. (2) yielding emittance estimate (b), (d), and (f). Representative electron beam spectrum measured using a calibrated spectrometer (g).

of the dogleg, is in good agreement with energy values determined from the calibrated spectrometer [Fig. 3(g)].

Generally, to establish spectrometer resolution, the dispersion free beam size in the dispersed plane should be known. Naturally, it cannot be measured while the beam is being dispersed. However, because of the inherent radial symmetry of the APL, it is reasonable to assume the focusing in the dispersed plane is identical to that in the nondispersed plane, and thus, the dispersion free beam size at each energy slice is the same in both planes. Furthermore, with small bend angles in the dogleg, we can safely ignore edge focusing effects in the dipoles themselves. Consequently, we can use the measured energy resolved beam size in the out-of-bend plane as a proxy to estimate the spectrometer resolution. With the smallest measured beam sizes of  $20\ \mu\text{m}$  and  $4\ \text{mm}$  dispersion, the resolution is 0.5% near the central energy. Away from the focused energy, the resolution generally gets worse due to the increase in the beam size. At the lower energies, this is partially compensated as the dispersion also increases, whereas at higher energies, the resolution degradation is compounded by decreasing dispersion. At the highest energies within the window of the measurements [Figs. 3(a), 3(c), and 3(e)], the resolution increases to 2%.

Beyond allowing a means to estimate the spectrometer resolution, the measured energy resolved beam size also intrinsically provides a means to estimate the source emittance in the nonbend plane. This method was demonstrated in Refs. 26–28 in which conventional quadrupoles were used as a focusing element, rather than an APL. Fitting the measurement to a model of the transport based on Eq. (2) yields the initial source size, divergence, and emittance over an energy slice of the bunch. In this context, the energy slice refers to the energy bandwidth included in the fit, which, in this case, is roughly 25%. The results of this fitting technique are shown in Figs. 3(b), 3(d), and 3(f) with values for the normalized emittance in the range of  $4\text{--}5\ \mu\text{m}$ . The uncertainty on each of these individual single shot measurements is roughly  $-1/+2\ \mu\text{m}$ . The uncertainty arises primarily from the determination of the beam size at each individual energy bin. At each energy, the beam size is determined by fitting a Gaussian to the lineout after thresholding it at 50% of the peak value. However, because of the existence of tails in the lineouts, thresholding at different percentages of the peak value will result in slightly different values for the beam size and, thus, different values for the emittance. We use the emittance values determined from thresholding at 25% and 75% to express this uncertainty.

The above measurements are enabled through the use of a replenishable LCPM<sup>15</sup> located 11 cm downstream of the target, which is used to separate the high intensity laser pulse from the electron beam. Using a plasma mirror allows the APL to be placed just 22 cm downstream of the target with a minimal risk of damage from the PW pulse. The specific advantage of using LCPMs, however, is that the films are typically only a few tens of nm thick, a factor of nearly 1000 reduction in the thickness compared to other thin materials used for plasma mirrors like VHS tape, Kapton, or Mylar.<sup>29</sup> The reduction in the thickness has a major impact on the preservation of emittance. Contributions to the emittance arising from well-known Coulomb scattering effects<sup>30</sup> can be estimated using basic principles of beam optics.<sup>31</sup> Essentially, the scattering material contributes an effective emittance that depends on the properties of the e-beam at the scattering interface, which is then added in quadrature to the source emittance.

In Fig. 4, the contribution to the normalized emittance for a scatterer located 11 cm downstream of a point source-like e-beam is

calculated for varying thicknesses of a carbon-based scatterer. Note that if the initial divergence of the electron beam is fixed, the contribution of the scatterer to the normalized emittance is independent of energy. This plot gives a good intuition on the limits a plasma mirror imposes. If the scatter emittance contribution is much less than the source emittance, there will be negligible degradation of the beam. On the other hand, if the scatter emittance is equal to or greater than the source emittance, there will be substantial dilution of the emittance and any measurement of the emittance downstream will only be a measure of the scatter emittance and not the source. Notably, even for a  $20\ \mu\text{m}$  Kapton film and a  $0.4\ \text{mrad}$  source, the emittance contribution is nearly  $10\ \mu\text{m}$ . For a  $20\ \text{nm}$  liquid crystal, that contribution drops to nearly  $0.1\ \mu\text{m}$ . Accordingly, the measured emittance values of  $4\text{--}5\ \mu\text{m}$  presented here are largely unaffected by any scattering effects from the plasma mirror. However, the use of tape drive style plasma mirrors loaded with Kapton or Mylar like ones used in previous experiments<sup>13,18</sup> would have prevented the resolution of such small emittances.

While reducing the plasma mirror thickness from tens of  $\mu\text{m}$  to tens of nm eliminates the most restrictive limit on emittance resolution, it is important to consider other limitations. For example, wakefields driven by the e-beam passing through the plasma can induce emittance growth related to head-to-tail focusing variation, which depends on the charge density of the beam at the APL as well as the density and length of the APL itself.<sup>17,32</sup> Although the bunch length of the electron beams produced here is not measured, we can reasonably assume that they are lower than the plasma wavelength associated with the LPA target ( $\approx 10\ \mu\text{m}$ ). Using this approximation, we note that for the work presented here, emittance dilution from self-driven wakefields inside of the APL is very likely lower than the smallest measured values of  $4\text{--}5\ \mu\text{m}$ . Nonetheless, wakefield effects should always be carefully considered for all future diagnostic applications involving APLs.

Another consideration is nonlinear focusing fields that may arise in the APL due to temperature gradients in the plasma.<sup>17</sup> Near the cold walls of the capillary, the current density drops and the magnetic field gradient becomes weaker, which can lead to emittance growth if the electron beam extends transversely far beyond the axis of the APL. However, if the rms beam size in the APL is less than  $R_{\text{APL}}/5$ , where  $R_{\text{APL}}$  is the radius of the APL, then the emittance is largely unaffected. In the context of the presented data, the generated e-beams have relatively low divergence ( $\sim 0.2$  to  $0.3\ \text{mrad rms}$ ). With the APL located

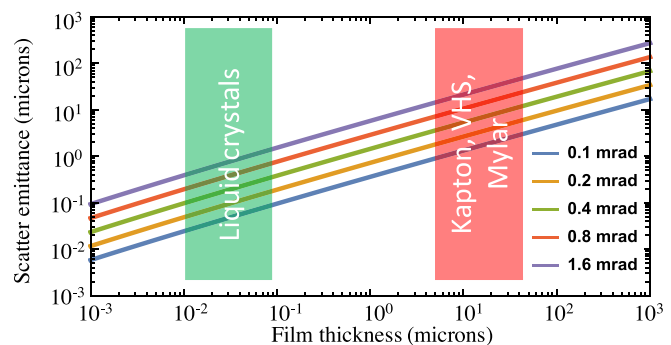


FIG. 4. Normalized emittance contribution from a scatterer of varying thicknesses located 11 cm downstream of the point source electron beam. Thin liquid crystal films offer several orders of magnitude improvement compared to thin solid state materials.

22 cm downstream of the LPA target, the beam grows to a transverse size of about 50–75  $\mu\text{m}$  rms at the APL entrance. With an APL diameter of 500  $\mu\text{m}$ , the impact of nonlinear fields can be largely avoided. Of course, it is possible that pointing fluctuations could result in the e-beam entering the APL off-axis, in which case, the beam will be more affected by the nonlinear fields. We also note that the primary effect of the nonlinear fields on the focused beam is the development of tails in the distribution. As discussed above, the beam size at each energy bin is determined by fitting a Gaussian after applying a threshold. The level of the threshold determines the relative contribution of the tails to the final emittance estimation. In this sense, the error bars included here for the emittance include contributions that may arise due to nonlinear focusing forces that can be found in APLs.

It should be noted that it was recently shown that the nonlinear focusing effect in APLs is the strongest when using light gas species like hydrogen and can be effectively eliminated by using heavier gas species like argon.<sup>32</sup> For this reason, future iterations of APL-based diagnostics should strongly consider using heavier gas species.

As final consideration on external influences on the measured emittance, we estimate the impact of scattering from the APL plasma itself. This estimate is based on the approach discussed in Ref. 8, which was generalized for mismatched beams. We estimate the emittance term associated with this scattering to be 0.3–0.6  $\mu\text{m}$ . Note that this scatter emittance term is added in quadrature to the source emittance to find the final emittance, which, with measured emittances in the range of 4–5  $\mu\text{m}$ , is a negligible contribution (a few tens of nm). Nonetheless, it is important to consider these scattering effects as they can impact the overall emittance resolution of the diagnostic, particularly if sub-1  $\mu\text{m}$  resolution is desired. These scattering effects can be considerably reduced by using shorter APLs, minimizing the distance between the LPA source and the APL, as well as using lower fill pressures in the APL.

This work has strong implications for the future of high energy LPA sources and their applications. Practical implementations of emerging technologies like the APL and LCPMs are fundamental to enhancing the capabilities of advanced compact accelerators. Here, we have shown one example in which we developed an ultra-compact magnetic spectrometer capable of providing sub-percent energy resolution for GeV class electron beams while simultaneously allowing single-shot emittance measurements.

This work was supported by the U.S. Department of Energy (DOE), Office of Science, Offices of High Energy Physics and Basic Energy Sciences, under Contract No. DE-AC02-05CH11231, the DOE Office of Science, Fusion Energy Sciences under Contract No. DE-SC0018192, the LaserNetUS initiative at the Bella Center, and the Gordon and Betty Moore Foundation under Grant No. GBMF4898. The contributions of W. P. Leemans to this research were made prior to his new position at DESY in February 2019.

## DATA AVAILABILITY

The data that support the findings of this study are available from the corresponding author upon reasonable request.

## REFERENCES

- <sup>1</sup>T. Tajima and J. M. Dawson, *Phys. Rev. Lett.* **43**, 267 (1979).
- <sup>2</sup>E. Esarey, C. B. Schroeder, and W. P. Leemans, *Rev. Mod. Phys.* **81**, 1229 (2009).
- <sup>3</sup>K. Nakajima, *Nat. Phys.* **4**, 92 (2008).
- <sup>4</sup>A. R. Maier, A. Meseck, S. Reiche, C. B. Schroeder, T. Seggebrock, and F. Grüner, *Phys. Rev. X* **2**, 031019 (2012).
- <sup>5</sup>Z. Huang, Y. Ding, and C. B. Schroeder, *Phys. Rev. Lett.* **109**, 204801 (2012).
- <sup>6</sup>R. Hajima, N. Kikuzawa, N. Nishimori, T. Hayakawa, T. Shizuma, K. Kawase, M. Kando, E. Minehara, H. Toyokawa, and H. Ohgaki, *Nucl. Instrum. Methods Phys. Res., Sect. A* **608**, S57 (2009).
- <sup>7</sup>O. Tesileanu, D. Ursescu, R. Dabu, and N. V. Zamfir, *J. Phys.* **420**, 012157 (2013).
- <sup>8</sup>C. B. Schroeder, E. Esarey, C. G. R. Geddes, C. Benedetti, and W. P. Leemans, *Phys. Rev. Spec. Top.-Accel. Beams* **13**, 101301 (2010).
- <sup>9</sup>A. Cianchi, M. P. Anania, M. Bellaveglia, M. Castellano, E. Chiadroni, M. Ferrario, G. Gatti, B. Marchetti, A. Mostacci, R. Pompili *et al.*, *Nucl. Instrum. Methods Phys. Res., Sect. A* **720**, 153 (2013).
- <sup>10</sup>K. Nakamura, W. Wan, N. Ybarrolaza, D. Syversud, J. Wallig, and W. P. Leemans, *Rev. Sci. Instrum.* **79**, 053301 (2008).
- <sup>11</sup>M. C. Downer, R. Zgadzaj, A. Debus, U. Schramm, and M. C. Kaluza, *Rev. Mod. Phys.* **90**, 035002 (2018).
- <sup>12</sup>W. K. H. Panofsky and W. R. Baker, *Rev. Sci. Instrum.* **21**, 445 (1950).
- <sup>13</sup>J. van Tilborg, S. Steinke, C. G. R. Geddes, N. H. Matlis, B. H. Shaw, A. J. Gonsalves, J. V. Huijts, K. Nakamura, J. Daniels, C. B. Schroeder *et al.*, *Phys. Rev. Lett.* **115**, 184802 (2015).
- <sup>14</sup>K. Nakamura, H. S. Mao, A. J. Gonsalves, H. Vincenti, D. E. Mittelberger, J. Daniels, A. Magana, C. Toth, and W. P. Leemans, *IEEE J. Quantum Electron.* **53**, 1–21 (2017).
- <sup>15</sup>P. L. Poole, A. Krygier, G. E. Cochran, P. S. Foster, G. G. Scott, L. A. Wilson, J. Bailey, N. Bourgeois, C. Hernandez-Gomez, D. Neely *et al.*, *Sci. Rep.* **6**, 32041 (2016).
- <sup>16</sup>J. B. Rosenzweig, *Fundamentals of Beam Physics* (Oxford University Press, 2003).
- <sup>17</sup>J. van Tilborg, S. K. Barber, C. Benedetti, C. B. Schroeder, F. Isono, H. E. Tsai, C. G. R. Geddes, and W. P. Leemans, *Phys. Plasmas* **25**, 056702 (2018).
- <sup>18</sup>S. Steinke, J. van Tilborg, C. Benedetti, C. G. R. Geddes, C. B. Schroeder, J. Daniels, K. K. Swanson, A. J. Gonsalves, K. Nakamura, N. H. Matlis *et al.*, *Nature* **530**, 190 (2016).
- <sup>19</sup>C. A. Lindstrom and E. Adli, *Phys. Rev. Accel. Beams* **19**, 071002 (2016).
- <sup>20</sup>C. A. Lindstrom, E. Adli, G. Boyle, R. Corsini, A. E. Dyson, W. Farabolini, S. M. Hooker, M. Meisel, J. Osterhoff, J. H. Röckemann *et al.*, *Phys. Rev. Lett.* **121**, 194801 (2018).
- <sup>21</sup>R. Pompili, M. P. Anania, M. Bellaveglia, A. Biagioni, S. Bini, F. Bisesto, E. Brentegani, F. Cardelli, G. Castorina, E. Chiadroni *et al.*, *Phys. Rev. Lett.* **121**, 174801 (2018).
- <sup>22</sup>J. H. Röckemann, L. Schaper, S. K. Barber, N. A. Bobrova, G. Boyle, S. Bulanov, N. Delbos, K. Floettmann, G. Kube, W. Lauth *et al.*, *Phys. Rev. Accel. Beams* **21**, 122801 (2018).
- <sup>23</sup>A. F. Pousa, A. M. de la Ossa, R. Brinkmann, and R. W. Assmann, *Phys. Rev. Lett.* **123**, 054801 (2019).
- <sup>24</sup>A. J. Gonsalves, K. Nakamura, J. Daniels, H.-S. Mao, C. Benedetti, C. B. Schroeder, C. Tóth, J. van Tilborg, D. E. Mittelberger, S. S. Bulanov *et al.*, *Phys. Plasmas* **22**, 056703 (2015).
- <sup>25</sup>J. van Tilborg, S. K. Barber, H. E. Tsai, K. K. Swanson, S. Steinke, C. G. R. Geddes, A. J. Gonsalves, C. B. Schroeder, E. Esarey, S. S. Bulanov *et al.*, *Phys. Rev. Accel. Beams* **20**, 032803 (2017).
- <sup>26</sup>R. Weingartner, S. Raith, A. Popp, S. Chou, J. Wenz, K. Khrennikov, M. Heigoldt, A. R. Maier, N. Kajumba, M. Fuchs *et al.*, *Phys. Rev. Spec. Top.-Accel. Beams* **15**, 111302 (2012).
- <sup>27</sup>S. K. Barber, J. van Tilborg, C. B. Schroeder, R. Lehe, H. E. Tsai, K. K. Swanson, S. Steinke, K. Nakamura, C. G. R. Geddes, C. Benedetti *et al.*, *Phys. Rev. Lett.* **119**, 104801 (2017).
- <sup>28</sup>N. Vafaie-Najafabadi, W. An, C. E. Clayton, C. Joshi, K. A. Marsh, W. B. Mori, E. C. Welch, W. Lu, E. Adli, J. Allen *et al.*, *Plasma Phys. Controlled Fusion* **58**, 034009 (2016).
- <sup>29</sup>B. H. Shaw, S. Steinke, J. van Tilborg, and W. P. Leemans, *Phys. Plasmas* **23**, 063118 (2016).
- <sup>30</sup>M. Tanabashi and P. D. Group, *Phys. Rev. D* **98**, 030001 (2018).
- <sup>31</sup>M. B. Reid, *J. Appl. Phys.* **70**, 7185 (1991).
- <sup>32</sup>C. A. Lindström and E. Adli, [arXiv:1802.02750](https://arxiv.org/abs/1802.02750) (2018).